Revealing the intricate dune-dune interactions of bidisperse barchans

An edited version of this paper was published by AGU. Copyright (2021) American Geophysical Union. Assis, W. R., Cúñez, F. D. and Franklin, E. M. (2022). Revealing the intricate dune-dune interactions of bidisperse barchans. Journal of Geophysical Research: Earth Surface, 127, e2021JF006588. https://doi.org/10.1029/2021JF006588
To view the published open abstract, go to https://doi.org/10.1029/2021JF006588.

W. R. Assis[1], F. D. Cúñez[2], E. M. Franklin[1]

[1]School of Mechanical Engineering, UNICAMP - University of Campinas, Rua Mendeleyev, 200, Campinas, SP, Brazil
[2]Department of Earth and Environmental Sciences, University of Rochester, Rochester, NY 14627, USA

Key Points:

- Two-species barchan-barchan interactions vary with the relative concentrations of each species
- We found configurations distinct from the one-species case, including a collision in which the upstream barchan is the largest
- We propose a timescale for the interactions of both monodisperse and bidisperse barchans

Corresponding author: Erick M. Franklin, `erick.franklin@unicamp.br`

Abstract

Three dimensional dunes of crescentic shape, called barchans, are commonly found on Earth and other planetary environments. In the great majority of cases, barchans are organized in large fields in which corridors of size-selected barchans are observed, and where barchan-barchan interactions play an important role in size regulation. Previous studies shed light on the interactions between barchans by making use of monodisperse particles, but dunes in nature consist, however, of polydisperse grains. In this paper, we investigate the binary interactions of barchans consisting of (i) bidisperse mixtures of grains and (ii) different monodisperse grains (one type for each barchan). We performed experiments in a water channel where grains of different sizes were poured inside forming two barchans that interacted with each other while filmed by a camera, and we obtained their morphology from image processing. We observed that a transient stripe appears over the dunes in cases of bidisperse mixtures, that interaction patterns vary with concentrations, and that different interactions exist when each barchan consists of different monodisperse grains. Interestingly, we found the conditions for a collision in which the upstream barchan is larger than the downstream one, and we propose a timescale for the interactions of both monodisperse and bidisperse barchans. Our results represent a new step toward understanding complex barchanoid structures found on Earth, Mars and other celestial bodies.

Plain Language Summary

Barchans are crescent-shaped dunes commonly found in dune fields on Earth and other planetary environments, and it has been shown that their sizes are highly influenced by barchan-barchan interactions. The composition of the granular bed can affect the observed patterns and sizes, but had not been investigated until now. Because those interactions take long times to be completed in gaseous environments (estimated in decades and millennia for dunes on terrestrial and Martian deserts, respectively) when compared with the aquatic case (of the order of minutes), we performed experiments in a water channel where two species of grains (in terms of size) were poured inside, forming two barchans that interacted with each other. We found different structures, including a collision in which the upstream barchan is the largest, and propose a timescale for the interactions of barchans. The identification of such timescale represents a new step for predicting the duration of barchan-barchan interactions and, more generally, scaling the evolution of dune fields on Earth, Mars and other planetary environments.

1 Introduction

Under one-directional fluid flow and limited amount of sand, three dimensional dunes of crescentic shape, called barchans, consistently grow (Bagnold, 1941; Herrmann & Sauermann, 2000; Hersen, 2004), being commonly found on Earth, Mars, other celestial bodies (Elbelrhiti et al., 2005; Claudin & Andreotti, 2006; E. J. R. Parteli & Herrmann, 2007). In the great majority of cases, barchans are organized in large fields in which corridors of size-selected barchans are observed, and where barchan-barchan interactions play an important role in size regulation (Hersen et al., 2004; Hersen & Douady, 2005; Kocurek et al., 2010; Génois, Hersen, et al., 2013; Génois, du Pont, et al., 2013; Assis & Franklin, 2020, 2021). Given the ubiquitous nature of barchans, understanding how their shape is formed, how they self-organize in regular fields, and how they are affected by the bed granulometry are of paramount importance to deduce the past and predict the future of barchans on Earth and other planetary environments.

Several studies investigated the interactions between barchans, shedding light on certain aspects of barchan-barchan interactions, but leaving many others, however, poorly understood. One of the drawbacks of previous studies is that field measurements were very limited in time, since aeolian barchans take decades to interact completely with each

other (Bagnold, 1941; Hersen et al., 2002). Field measurements of aeolian barchan-barchan interactions are of course important, since they measure processes happening in nature, and previous studies showed that the collisions of barchans regulate their size and generate different barchanoid forms (Norris & Norris, 1961; Gay, 1999; Vermeesch, 2011; Elbelrhiti et al., 2008; Hugenholtz & Barchyn, 2012). However, the time series are frequently incomplete, and, therefore, numerical and experimental investigations have been conducted in parallel with field experiments. Another drawback is that previous experimental and numerical studies made use of monodisperse particles (unimodal distribution), whereas dunes in nature consist of polydisperse grains (heterogenous grain sizes). One way to overcome those drawbacks is by carrying out experiments with polydisperse grains under water, the subaqueous barchans being much faster and smaller than the aeolian dunes (the former having characteristic lengths and turnover times of centimeters and minutes, e.g., Hersen et al., 2002; Franklin & Charru, 2009, 2011; Alvarez & Franklin, 2017).

The numerical studies made use of continuum (Schwämmle & Herrmann, 2003; Durán et al., 2005; Zhou et al., 2019) and discrete (Katsuki et al., 2011) models to compute the evolution of a bed surface into a dune field, most of them incorporating rules for barchan-barchan interations (Lima et al., 2002; E. Parteli & Herrmann, 2003; Katsuki et al., 2005; Durán et al., 2009). In addition to these techniques, Durán et al. (2009) and Génois, du Pont, et al. (2013) proposed an agent-based model that makes use of sand- flux balances and elementary rules for barchan collisions, and Bo and Zheng (2013) used a scale-coupled model (Zheng et al., 2009) to obtain the probability of occurrence of different types of barchan-barchan collisions. Those numerical investigations showed that barchan-barchan collisions lead to corridors of size-selected barchans, pointing toward homogeneous dune fields. However, model simplifications prevented them from reproducing correctly all barchan-barchan interactions, and, in addition, there is a lack of numerical studies at the grain scale (which could give important information for understanding binary interactions, such as mass transfers between dunes, diffusion of grains within one barchan, and motion of grains over the barchan surface).

The experiments were carried out almost exclusively in water tanks and channels. Some studies measured the flow disturbances caused by an upstream barchan upon a downstream one, such as was done by Bristow et al. (Bristow et al., 2018, 2019, 2020), who found, among other findings, that turbulence levels increase on the stoss surface of the downstream dune, enhancing erosion over the downstream dune. Other investigations measured the evolution of two interacting bedforms, identifying different interaction patterns (Endo et al., 2004; Hersen & Douady, 2005; Bacik et al., 2020; Assis & Franklin, 2020) and mass exchanges at the grain scale (Assis & Franklin, 2021). Endo et al. (2004) investigated collisions of aligned barchans by varying their mass ratio while maintaining fixed the water flow rate, initial conditions and grain types, and they found three collision patterns which were called merging, exchange and fragmentation-chasing by Assis and Franklin (2020) (and explained next). Hersen and Douady (2005) investigated the collisions of off-centered barchans by varying their transverse distances while keeping the other parameters fixed, and showed that collisions produce smaller barchans, regulating thus their size when in a barchan field. The experiments of Bacik et al. (2020) were devoted to the interaction over long times between a pair of two-dimensional dunes in a circular channel, and they found that turbulent structures of the disturbed flow prevent dune collisions by inducing dune-dune repulsion. Recently, Assis and Franklin (2020, 2021) inquired further into the binary interactions of subaqueous barchans by conducting experiments in both aligned and off-centered configurations where the water flow rates, grain types (diameter, density and roundness), pile masses, longitudinal and transverse distances, and initial conditions were varied, and measurements were made at the bedform and grain scales. They found five interaction patterns for both aligned and off-centered configurations, proposed classification maps, measured the trajectories of individual grains during barchan-barchan interactions, and found the typical lengths and velocities of grains, the mass exchanged between barchans, and a diffusive length for some collisions.

From the previous works, the most comprehensive classification of barchan-barchan interactions is the one presented in Assis and Franklin (2020), which identifies: (i) chasing, when collision does not occur, the upstream barchan not reaching the downstream one; (ii) merging, when collision occurs and the dunes merge; (iii) exchange, when, once collision takes place, a small barchan is ejected; (iv) fragmentation-chasing, when the downstream dune splits without collision taking place and the downstream bedforms outrun the upstream one; and (v) fragmentation-exchange, when fragmentation initiates, collision takes place, and a small barchan is ejected. The question that persists is if the same patterns and classification maps proposed by Assis and Franklin (2020) remain valid for aeolian and Martian barchans (and also other planetary environments), and polydisperse dunes. While proving the validity for aeolian and Martian barchans is hindered by their large timescales, that for polydisperse barchans, on the other hand, can be investigated in the subaqueous case.

Concerning dunes of polydisperse grains, Alvarez et al. (2021) investigated experimentally the growth of subaqueous single barchans consisting of bidisperse grains (bimodal distribution). In their experiments, single granular piles consisting of bidisperse mixtures in terms of grain sizes and/or densities were developed into barchan dunes, and they found that, depending on the mixed grains, either (i) denser, (ii) smaller, or (iii) smaller and less dense grains tend to accumulate over the barchan surface. They also found that a transient stripe transverse to the flow direction appears just upstream the crest of the initial bedform and migrates toward its leading edge until disappearing, that that line separates a downstream region where segregation is complete from the upstream region where segregation is still occurring, and that the final barchan morphology is roughly the same as that of monodisperse barchans. Finally, they proposed that segregation patterns result from a competition between fluid entrainment and ease of rolling, and showed that grains segregate with a diffusion-like mechanism.

Although previous studies explained certain aspects of barchan-barchan interactions, such as the existing patterns, their classification in parameter spaces, and sand redistribution during interactions, many others remain to be understood. Among the major questions still to be investigated, there are the interactions between barchans in the presence of polydispese (heterogeneous) grains and the identification of timescales for barchan-barchan interactions. While the first better represents dunes in the field, the latter imply a measurement unit for durations of dune-dune interactions.

In this paper, we investigate the binary interactions of barchans when grains of two different sizes are involved, which is a simplified case of real dunes consisting of polydisperse grains. For that, we inquired into two specific cases: (i) each bedform consisting of bidisperse mixtures (bimodal distributions of grains); (ii) each bedform consisting of a given, but different between them, grain type (two-species monodisperse barchans). The experiments were conducted in a water channel where grains were poured inside, forming two conical piles that were afterward deformed by the water flow into barchans that interacted with each other. The evolution and interactions of bedforms were recorded by a conventional camera and their morphology was obtained from image processing. We observe that a transient stripe appears over the dunes in cases of bidisperse mixtures, just as happens for single bidisperse barchans (Alvarez et al., 2021). We show, for the first time, that interaction patterns vary with grain concentrations, and that different interactions exist when each barchan consists of different monodisperse grains (two-species monodisperse barchans), including collisions in which the upstream barchan is larger than the downstream one. Finally, we propose a timescale for the interactions of barchans valid not only for the two-species cases (cases i and ii), but also when only one species is involved (one-species monodisperse barchans). Our results represent a new step toward understanding complex barchanoid structures found on Earth, Mars and other celestial bodies.

In the following, Section 2 describes the experimental setup and procedure, Section 3 presents the obtained results, and Section 4 presents the conclusions.

2 Experimental Setup

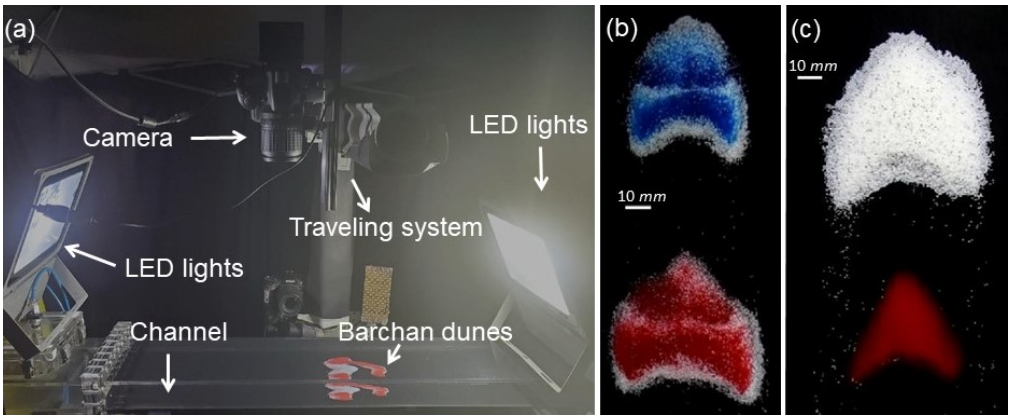

Figure 1. (a) Photograph of test section showing the dunes, camera and LED lights; (b) top-view image of two interacting bidisperse barchans (case *e* of Table 1); (c) top-view image of two interacting monodisperse barchans of different granulometry (case *o* of Table 1, of a larger barchan reaching a smaller one); In figures (b) and (c) the flow is from top to bottom.

The experimental device consisted basically of a water tank, centrifugal pumps, a flow straightener, a 5-m-long closed-conduit channel, a settling tank, and a return line, so that we imposed a pressure-driven water flow in closed loop. The channel had a rectangular cross section 160 mm wide by $2\delta = 50$ mm high, was made of transparent material, and consisted of a 3-m-long entrance section (corresponding to 40 hydraulic diameters), a 1-m-long test section, and a 1-m-long section connecting the test section to the channel exit. With the channel filled with water in still conditions, controlled grains were poured inside in order to form two aligned piles consisting of (i) bidisperse mixtures (bimodal distributions); (ii) different monodisperse (unimodal) grains (two-species, each pile consisting of one single species). In the case of bidisperse mixtures, the grains were weighted in the desired proportions and mixed before being poured. Afterward, a specified water flow was imposed, deforming each pile into a barchan dune that interacted with each other while a camera recorded top view images of the bedforms. No influx of grains coming from regions upstream the test section was imposed and, therefore, the entire system decreased in mass along time. Using the same terminology of previous works (Assis & Franklin, 2020, 2021), we call *impact barchan* the one that was initially upstream and *target barchan* the one that was initially downstream. Figure 1a shows a photograph of the test section, and Figures 1b and 1c top-view images of two interacting barchans consisting each of bidisperse and monodisperse grains, respectively. The layout of the experimental device is shown in the supporting information.

In our tests, we used tap water at temperatures within 22 and 28 °C and round glass beads ($\rho_s = 2500$ kg/m^3) with diameters 0.15 mm $\leq d_{s1} \leq$ 0.25 mm and 0.40 mm $\leq d_{s2} \leq$ 0.60 mm, which we call species 1 and 2, respectively. We consider in our computations the mean values $d_1 = 0.2$ mm and $d_2 = 0.5$ mm of d_{s1} and d_{s2}, respectively, and we used grains of different colors (white, red and blue) in order to track the different species along images (all grains have the same density, see the supporting information for microscopy images of the used grains). We varied the concentration of each grain

type (ϕ_1 and ϕ_2) between 0 and 1, the mass ratio of the piles (initial mass of the impact barchan m_i divided by that of the target one m_t) between 0.02 and 4, and the water velocities within 0.278 m/s $\leq U \leq$ 0.347 ms, where U is the cross-sectional mean velocity of water. These values correspond to Reynolds numbers based on the channel height, $Re = \rho U 2\delta/\mu$, within 1.39×10^4 and 1.74×10^4, where μ is the dynamic viscosity and ρ the density of the fluid. We computed shear velocities of the undisturbed water flow over the channel walls u_* from measurements with a two-dimensional two-component particle image velocimetry (2D2C-PIV) device, and we use u_* as a reference value for fluid shearing even when bedforms are present in the channel. Our measurements show values within 0.0159 and 0.0193 m/s and that u_* follows the Blasius correlation (Schlichting, 2000). With those values, the Shields number $\theta = (\rho u_*^2)/((\rho_s - \rho)gd)$ varied within 0.034 and 0.127 (where g is the acceleration of gravity), and the particle Reynolds number Re_* $= \rho u_* d/\mu$ within 3 and 10. Because we are interested in the short-range interaction of barchans, the initial separation Δx_d was kept close to the diameter of the impact bedform D_i, with some deviations due to the preparation of initial piles (Assis and Franklin (2020) varied considerably Δx_d and observed that the patterns remained the same, the only effect being the increase in the duration of the interactions). Table 1 summarizes the tested conditions, and complete tables with all the parameters (in dimensional form) are available on an open repository (Assis et al., 2021).

A digital camera with a lens of 18-140 mm focal distance and F2.8 maximum aperture was mounted on a traveling system in order to have a top view of the bedforms, and lamps of light-emitting diode (LED) were used as light source. The camera was of complementary metal-oxide-semiconductor (CMOS) type with a maximum resolution of 1920 px $\times$ 1080 px at 60 Hz, and the region of interest (ROI) was set between 1311 px $\times$ 451 px and 1920 px $\times$ 771 px, for fields of view varying within 354 mm $\times$ 122 mm and 507 mm $\times$ 122 mm. The acquired images were afterward processed by numerical scripts that identified and tracked bedforms and patterns, and were based on Crocker and Grier (1996). Movies showing collisions of bidisperse barchans are available in the supporting information and on an open repository (Assis et al., 2021).

3 Results and discussion

3.1 Bidisperse piles

We followed the barchans consisting of bidisperse mixtures, for different concentrations of species 1 and 2, and we found patterns similar to those found by Assis and Franklin (2020) for monodisperse (one-species) barchans. The obtained patterns are shown in Figure 2 for fixed concentrations $\phi_1 = 0.5$ and $\phi_2 = 0.5$ in both initial piles (cases a to e in Table 1), and in Figure 3 for concentrations ϕ_1 and ϕ_2 alternating between either 0.2 or 0.8 (cases f to k in Table 1). Movies for all cases are available on an open repository (Assis et al., 2021), and for cases b and o in the supporting information.

For $\phi_1 = \phi_2 = 0.5$, the same interaction patterns of one-species barchans occur (Assis & Franklin, 2020), namely the chasing, merging, exchange, fragmentation-chasing and fragmentation-exchange patterns (Figures 2e, 2a, 2b, 2d and 2c, respectively). By alternating ϕ_1 and ϕ_2 between either 0.2 or 0.8, using the same (Figures 3a, 3b, 3e and 3f, corresponding to cases f, g, j and k of Table 1) or inverted (Figures 3c and 3d, corresponding to cases h and i of Table 1) concentrations for the impact and target barchans, and for three values of m_i/m_t while all the other parameters were kept constant, we obtained the merging, exchange and fragmentation-exchange patterns. We note that it is probable that the chasing and fragmentation-chasing patterns exist also for the concentrations employed. We did not, however, vary the mass ratio in order to investigate this specifically.

Case	ϕ_{1t}	ϕ_{2t}	ϕ_{1i}	ϕ_{2i}	D_t	D_i	Δx_d	Re	u_*	m_i/m_t	t_s	t_c	Pat
...	...	...	...	...	mm	mm	mm	...	mm/s	...	s	...	...
a	0.5	0.5	0.5	0.5	63	18	18	1.56×10^4	0.0176	0.02	230	0.1	M
b	0.5	0.5	0.5	0.5	61	24	23	1.56×10^4	0.0176	0.05	450	0.2	E
c	0.5	0.5	0.5	0.5	56	27	20	1.56×10^4	0.0176	0.11	499	0.6	FE
d	0.5	0.5	0.5	0.5	43	30	30	1.56×10^4	0.0176	0.43	1537	∞	FC
e	0.5	0.5	0.5	0.5	52	48	39	1.56×10^4	0.0176	0.67	10637	∞	C
f	0.8	0.2	0.8	0.2	56	22	21	1.56×10^4	0.0176	0.05	482	0.1	E
g	0.2	0.8	0.2	0.8	60	25	21	1.56×10^4	0.0176	0.05	318	0.2	M
h	0.8	0.2	0.2	0.8	54	21	21	1.56×10^4	0.0176	0.05	215	0.2	E
i	0.2	0.8	0.8	0.2	55	21	23	1.56×10^4	0.0176	0.05	893	0.3	∼FE
j	0.8	0.2	0.8	0.2	53	26	28	1.56×10^4	0.0176	0.11	889	0.3	FE
k	0.2	0.8	0.2	0.8	59	30	34	1.56×10^4	0.0176	0.25	800	0.2	FE
l	1.0	0.0	0.0	1.0	44	49	39	1.56×10^4	0.0176	1.00	989	0.1	U
m	1.0	0.0	0.0	1.0	51	55	29	1.39×10^4	0.0159	1.00	870	0.5	U
n	1.0	0.0	0.0	1.0	57	43	34	1.56×10^4	0.0176	0.25	596	0.04	U
o	1.0	0.0	0.0	1.0	39	62	34	1.74×10^4	0.0193	4.00	1471	0.04	U

Table 1. Label of tested cases, initial concentration (mass basis) of each species within the target (ϕ_{1t} and ϕ_{2t}) and impact (ϕ_{1i} and ϕ_{2i}) piles, initial diameters of target and impact piles, D_t and D_i, respectively, initial separation Δx_d, channel Reynolds number Re, undisturbed shear velocity u_*, ratio between initial masses m_i/m_t, proposed timescale t_s (Eq. 4 in Subsection 3.3), characteristic time t_c (shown in Subsection 3.3), and interaction pattern Pat. C, M, E, FC, FE and U stand for chasing, merging, exchange, fragmentation-chasing, fragmentation-exchange and undefined patterns, respectively.

Although the bidisperse piles (mixtures) produce the same interaction patterns observed for one-species barchans, they present some peculiarities in terms of morphodynamics. Two of those peculiarities are related with grain segregation, as shown by Alvarez et al. (2021) for single barchans: the accumulation of the smaller grains over the surface of bedforms, and the appearance of a transient stripe (the narrow band consisting of large grains), transverse to the flow direction, that initiates upstream the crest of the initial bedform and migrates toward its leading edge until disappearing. Alvarez et al. (2021) showed that the transient stripe separates the region where segregation is complete from that where segregation is ongoing, and the same feature applies here since bidisperse conical piles are being deformed into bidisperse barchans. Another difference is the formation of a large void (absence of grains) when the impact barchan reaches the target one in the exchange pattern (Figures 2b and 3a, corresponding to cases *b* and *f* in Table 1). This void region occurs in the recirculation bubble of the impact barchan and persists until a baby barchan containing only grains from the target one is ejected. The baby barchan has roughly the same projected area of the impact barchan when $\phi_1 = \phi_2 = 0.5$, but not necessarily when $\phi_1 \neq \phi_2$, and, just after the baby barchan is ejected (at 157 s in Figure 2b and 155 s in Figure 3a), the parent bedform has an unusual shape, resembling two elongated barchans containing grains from the target barchan and linked by grains from the impact one. After some time, the parent bedform attains a barchan shape.

Figure 4a presents the time evolution of areas occupied by the void region A_{vd}, normalized by the total area (projected area) A_t occupied by grains, for the exchange cases when $\phi_1 = \phi_2 = 0.5$ (Figure 2b, case *b*) and $\phi_1 \neq \phi_2$ (Figure 3a, case *f*). The computation of areas began when the impact barchan reached the target one, forming a closed void, and finished when the void was no longer closed, the baby barchan being ejected

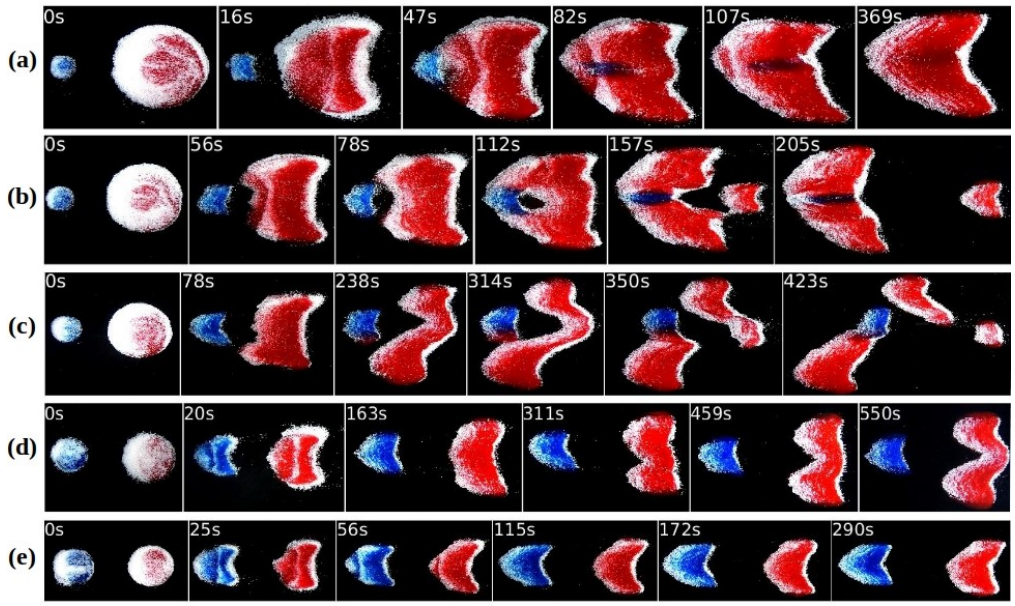

Figure 2. Snapshots of interactions of bidisperse barchans for fixed initial concentrations ϕ_1 = 0.5 and ϕ_2 = 0.5. In the snapshots, the white (clearer) beads correspond to d_2 = 0.5 mm and red and blue (darker) beads to d_1 = 0.2 mm, the water flow is from left to right, and the corresponding times are shown in each frame. Figures (a) to (e) correspond to cases *a* to *e* of Table 1: (a) merging; (b) exchange; (c) fragmentation-exchange; (d) fragmentation-chasing; (e) chasing.

just afterward (see the supporting information for examples of void region detection and the time evolution of A_{vd} in dimensional form). We observe that the void area corresponds to 5 to 10% of the projected area occupied by the grains, the void remaining roughly constant for a certain time and then increasing considerably by the time the baby barchan is to be ejected. We observe also that the void is greater when in the presence of a large concentration of smaller grains. The reasons and mechanisms by which the void is formed remain to be investigated further, but they seem associated with granulometric distributions, since we had not observed voids in our experiments with one-species barchans (Assis & Franklin, 2020, 2021).

As a consequence of the aforementioned differences, the resulting patterns in the bidisperse case do not necessarily occur under the same conditions as for monodisperse barchans. Figure 4b plots the experimental points measured with bidisperse barchans in the map proposed by Assis and Franklin (2020) for the aligned case (figure modified from Assis & Franklin, 2020), which is drawn in the parameter space consisting of the Shields number θ and dimensionless particle number $\xi_N = \Delta_N/\Sigma_N$, where Δ_N is the difference and Σ_N the sum of the number of grains forming each pile. For the bidisperse case (symbols in Figure 4b), θ of each pile was computed for each species (i.e., θ_1 and θ_2 using d_1 and d_2, respectively) and then averaged by the number of grains of each species: $\theta = N_1\theta_1/N + N_2\theta_2/N$, where $N1$, N_2 and N are the number of grains of species 1, 2, and their sum, respectively. In addition, for cases where impact and target barchans had different compositions (cases *h* and *i*), θ was afterward computed as an averaged weighted by the size (total number of grains) of each barchan. We observe that most of points fall within the corresponding patterns found in the monodisperse case, or very near the boundaries, but some of them deviate, crossing regions in the map. In general, while the exchange, fragmentation-chasing and fragmentation-exchange tend to remain within their

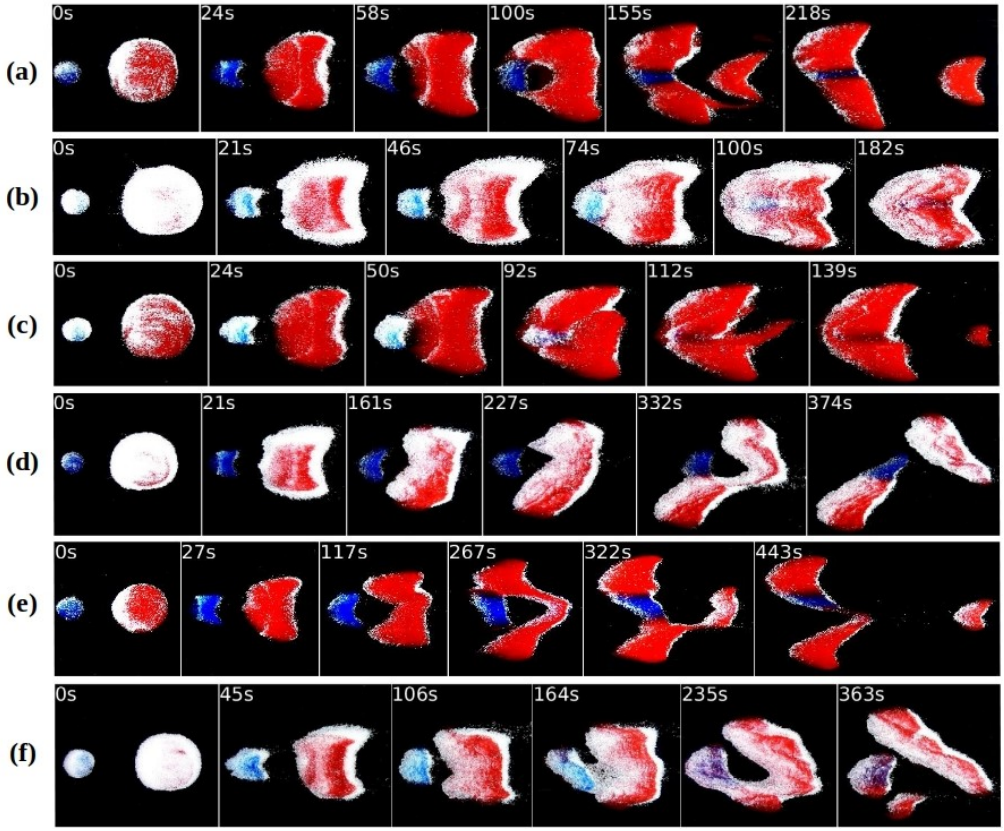

Figure 3. Snapshots of interactions of bidisperse barchans for fixed initial concentrations ϕ_1 and ϕ_2 alternating between either 0.2 or 0.8. In the snapshots, the white (clearer) beads correspond to $d_2 = 0.5$ mm and red and blue (darker) beads to $d_1 = 0.2$ mm, the water flow is from left to right, and the corresponding times are shown in each frame. Figures (a) to (f) correspond to cases f to k of Table 1: (a) exchange; (b) merging; (c) exchange; (d) fragmentation-exchange; (e) fragmentation-exchange; (f) fragmentation-exchange.

respective boundaries, the chasing and merging patterns deviate considerably, the former crossing the line and occupying part of the fragmentation-chasing region and the latter occupying part of the exchange region. We note that if we had used m_i/m_t or a length ratio (as other authors did, e.g., Endo et al., 2004; Katsuki et al., 2005, 2011; Génois, Hersen, et al., 2013) instead of ξ_N, many of the symbols would be superposed in Figure 4b even if measured patterns are different, since the mass ratio does not take into consideration details about granular compositions (see the supporting information for a map using m_i/m_t). This corroborates, in a certain way, the use of a dimensionless parameter based on the number of elements (ξ_N) rather than m_i/m_t.

In particular, we analyzed the projected areas occupied by grains during some exchange patterns. For monodisperse dunes, Assis and Franklin (2020, 2021) showed that the impact barchan first merges with the target one, and afterward a new barchan (baby barchan) is ejected (the remaining bedform being the parent barchan). In addition, Assis and Franklin (2020) showed that the baby barchan has roughly the same size of the impact barchan, but contains grains only from the target one. In the case of bidisperse mixtures, a similar behavior happens. Figure 5 shows the projected areas of bedforms during the exchange processes of Figures 2b, 3a and 3c (cases a, f and h, corresponding to

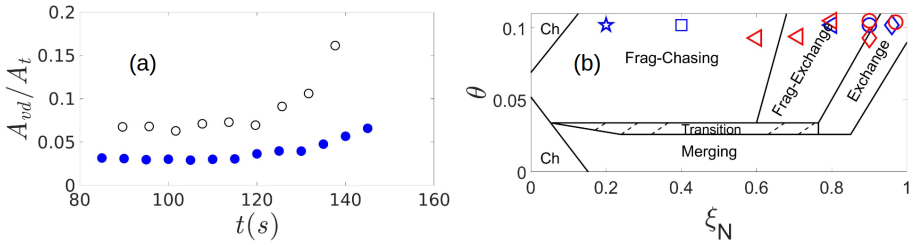

Figure 4. (a) Area occupied by the void region A_{vd} normalized by the total area (projected) A_t occupied by grains as a function of time. Solid blue circles correspond to the exchange pattern when $\phi_1 = \phi_2 = 0.5$ (Figure 2b, case b) and open black symbols when $\phi_1 \neq \phi_2$ (Figure 3a, case f). (b) Interaction patterns for barchans of bidisperse mixtures: classification map proposed by Assis and Franklin (2020) for monodisperse barchans, over which we superposed the experimentally obtained chasing - Ch ($\star$), merging ($\diamond$), exchange ($\circ$), fragmentation-chasing ($\square$), and fragmentation-exchange ($\triangleleft$) patterns for the bidisperse case. Blue color corresponds to $\phi_1 = \phi_2 = 0.5$ (Figure 2) and red to $\phi_1 \neq \phi_2$ (Figure 3). Figure modified from Assis and Franklin (2020).

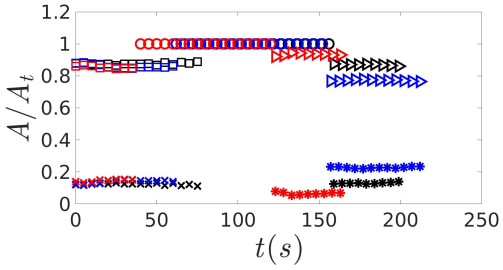

Figure 5. Projected areas, normalized by A_t, of impact (x), target ($\square$), merged ($\circ$), parent ($\triangleright$), and baby (*) barchans, respectively, as functions of time, during exchange processes. Black, blue and red colors correspond to cases a, f and h (Figures 2b, 3a and 3c), respectively.

black, blue and red colors, respectively. A graphic in dimensional form is available in the supporting information). While the baby barchan does not contain grains from the impact barchan (seen directly from Figures 2b, 3a and 3c), Figure 5 shows that their areas are roughly the same (for the analyzed cases).

In summary, we show that in the mixed case the interaction patterns and their dynamics are roughly the same as in the monodisperse case; however, although the maps proposed in Assis and Franklin (2020) bring valuable information for classifying the barchan-barchan interactions, results with polydisperse dunes can deviate from the proposed boundaries. Therefore, the distribution of grains within the barchans should be taken into consideration in analyses of barchan-barchan interactions occurring in nature.

3.2 Two-species monodisperse piles

We followed the initially monodisperse bedforms consisting each of different grains, and we found different patterns. These patterns, cases l to o in Table 1, are shown in Figure 6, which presents snapshots of barchans at some instants during their interactions, including a collision where the impact barchan was larger than the target one (see the supporting information or Assis et al. (2021) for movies of collisions). For this specific

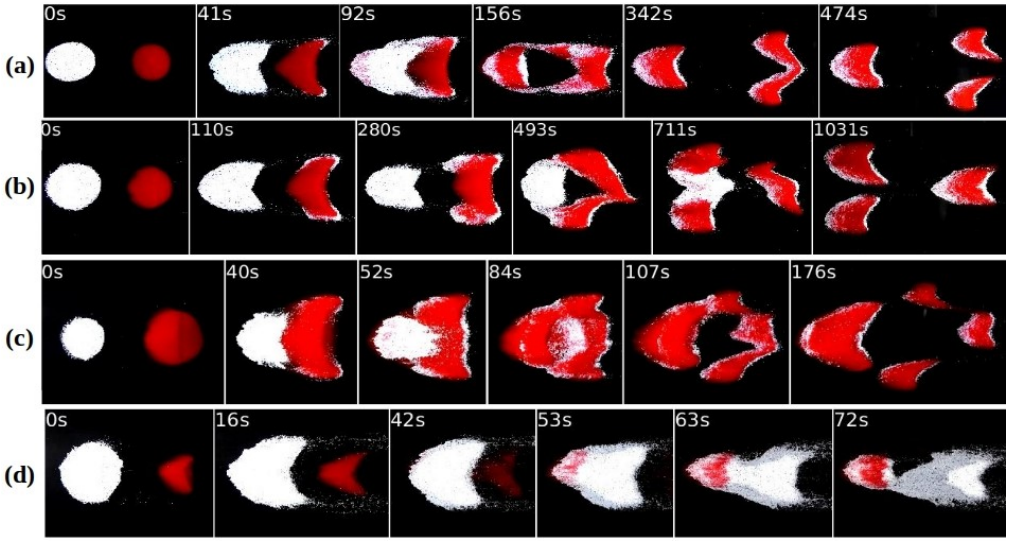

Figure 6. Snapshots of barchan interactions for initially monodisperse piles of different grains (two-species monodisperse piles). In the snapshots, the upstream pile consists of white (clearer) beads with $d_2 = 0.5$ mm and the downstream pile of red (darker) beads with $d_1 = 0.2$ mm, the water flow is from left to right, and the corresponding times are shown in each frame. Figures (a) to (d) correspond to cases *l* to *o* of Table 1.

case, we made use of larger grains in the impact dune since the celerity of barchans varies with the diameter of their grains (Franklin & Charru, 2011, see also Eq. 2 in Subsection 3.3).

For all the interactions shown in Figure 6, the impact barchan consisted of grains of species 2 ($d_2 = 0.5$ mm) in white color and the target barchan of species 1 ($d_1 = 0.2$ mm) in red color. In Figure 6a (case *l* in Table 1), the barchans collide, forming a large void in the recirculation region when they touch each other, and with the larger grains moving over the smaller ones that, in their turn, emerge at the toe of the resulting bedform (at 92 s). Afterward (at 156 s), the smaller grains having accumulated over the surface of the resulting bedform, the latter begins to split in what seems, initially, two barchans linked by two large branches. Finally (at 474s), they split in three barchans (one upstream and two downstream, in a staggered configuration) consisting each of bidisperse grains. Figures 7a and 7b show the time evolution of projected areas of dunes for cases *l* and *m*, respectively (Figures 7c and 7d in dimensionless form, normalized by A_t). Interestingly, we can observe from Figure 7a that, after the dunes collide (at ~ 90 s), the projected area of the resulting bedform first increases and then decreases. This is due, respectively, to larger grains migrating over the smaller ones and spreading over the dune, and afterward the smaller grains accumulating over the dune surface and decreasing the projected area. In addition, Figure 7a shows that the two final downstream barchans have roughly the same size.

In Figure 6b (case *m* in Table 1), the behavior is similar to that of Figure 6a, the main difference being that the final state is inversed: two upstream barchans and one downstream barchan, in a staggered configuration. In both cases *l* and *m* the initial masses are the same (the initial diameter of the impact pile being larger since it consists of larger grains), only the fluid velocity is different, being higher for case *l*. Why the behavior changes by changing the water velocity remains to be investigated (we do not advance an explanation for the moment). However, we can observe from Figure 7b the same increase and

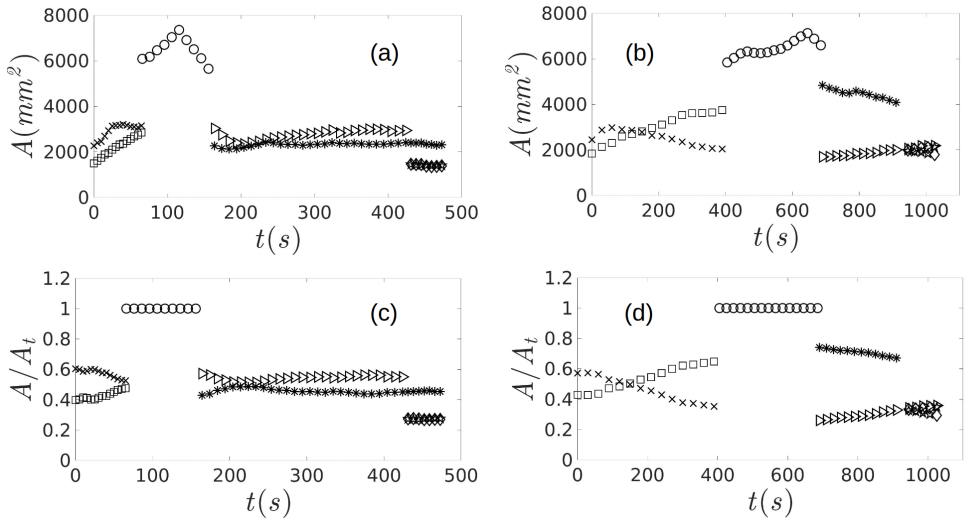

Figure 7. Projected areas of impact (x), target (□), merged (○), upstream after splitting (*), parent (▷), and baby barchans (◇ and ⋆), respectively, during undefined-exchange processes for (a) and (c) case *l* (Figure 6a) and (b) and (d) case *m* (Figure 6b). Figures (a) and (b) are in dimensional and (c) and (d) in dimensionless form (normalized by A_t).

decrease of the projected area after the dunes have collided (at $\sim$ 400 s), that the resultant bedform splits first in one larger upstream and one smaller downstream bedform (at $\sim$ 700 s), and that the upstream bedform splits in two dunes later (at $\sim$ 950 s). We end finally with three barchans of roughly the same size.

Figure 6c corresponds to case *n* of Table 1, and shows a collision in which three barchans are ejected from the merged bedform. This case resembles the exchange pattern (Assis & Franklin, 2020, 2021), with the difference that three baby barchans are ejected, one aligned and two in staggered configuration.

Finally, Figure 6d corresponds to case *o* of Table 1, the unusual case of a collision of a larger impact with a smaller target barchan. As far as we know, this is the first time that this kind of collision is reported (see the supporting information or Assis et al. (2021) for a movie of this interaction), Groh et al. (2009) having measured the collision of a larger upstream dune with a smaller downstream one, in the 2D case, by placing initially the latter in the recirculation region of the former, thus forcing collision (in addition to having, apparently, entrance effects in their test section). We observe that, as the impact barchan gets closer to the target one, the latter becomes more elongated, while grains leaving the horns of the impact barchan are entrained further downstream and are not incorporated by the target barchan. During the collision (t $\approx$ 48 s), the larger grains move over the smaller ones, which, in their turn, emerge at the toe of the resulting bedform. Finally, a monodisperse baby barchan consisting of only larger grains is ejected from the merged bedform (grains from the impact dune, different from all cases reported previously), resulting, in fact, of larger grains being entrained further downstream. The remaining grains form an upstream bidisperse barchan with smaller grains populating its upper surface.

Figure 8 shows the time evolution of projected areas occupied by white and red grains for case *o*. From Figure 8a, we observe an initial increase of both areas due to the spreading of the initial conical pile (being deformed into barchan dunes), with a time interval when areas remain roughly constant. When the larger dune approaches the smaller one,

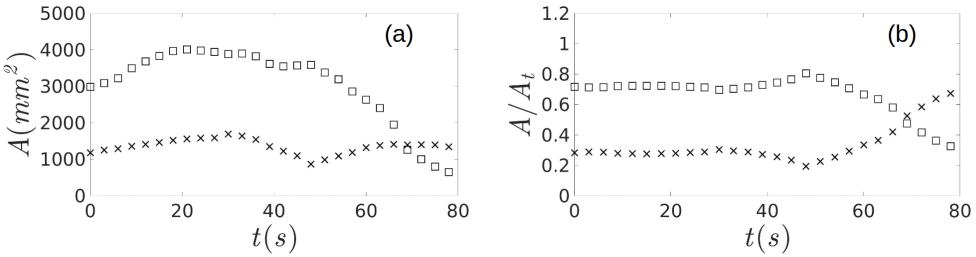

Figure 8. Time evolution of projected areas occupied by white (□) and red (x) grains for case *o* (Figure 6d), in (a) dimensional form and (b) normalized by A_t. OBS: the monolayer consisting of white grains observed in Figure 6d was neglected.

the vortex on the recirculation region of the former entrains grains from the latter toward its lee face. Because the larger grains move easier over the smaller ones (Alvarez et al., 2021), these remain on the bottom of the impact barchan until they emerge at the toe of the impact one, being again exposed to the fluid flow. When the dunes collide, the white grains then move over the red (smaller) ones, which appear at the toe of the resulting bedform. This "swallowing" process appears in Figure 8 as a decrease followed by an increase of the area occupied by red grains within 30 s $< t <$ 70 s. Finally, by the end of the collisional process ($t \approx 70$ s on), a greater number of larger (white) grains are exposed to the fluid flow and are either entrained further downstream or form a monolayer between both barchans, which makes the area occupied by the larger (white) grains to decrease considerably (the monolayer being neglected in Figure 8). By considering Figure 6d, we observe that a significant amount of larger (white) grains is entrained downstream (white grains leaving the horns, and also the reduction in the area occupied by the white grains).

In common for cases *l* to *o*, the larger grains move over the smaller ones, being entrained further downstream and/or accumulating on the lee face and forming a carpet for the smaller grains. The same mechanism proposed by Alvarez et al. (2021) seems to apply here, i.e., the segregation results from a competition between fluid entrainment and ease of rolling. Other than that, we do not advance more explanations for the patterns shown in Figure 6, but we propose, however, a timescale that applies to all cases investigated and is presented in Subsection 3.3.

3.3 Timescale

A question that remained to be answered for barchan-barchan interactions even in monodisperse conditions (Endo et al., 2004; Hersen & Douady, 2005; Assis & Franklin, 2020, 2021), and that can now be investigated for bidisperse barchans, is the existence of a proper timescale for the problem. In the following, we propose a timescale and evaluate it in the subaqueous case. A reasonable timescale for the binary interaction of dunes can be built as their initial separation Δx_d divided by their relative velocity ΔV_d,

$$t_s = \frac{\Delta x_d}{\Delta V_d} \tag{1}$$

where ΔV_d is the difference between the celerities V_d of impact and target barchans (at the beginning of the interaction), and t_s represents a typical time for the collision of barchans (faster for closer barchans with stronger relative velocities). Franklin and Charru (2011)

investigated the celerities of subaqueous barchans by varying water velocities, grain types, and dune sizes, and found that

$$\frac{V_d}{V_{ref}} = 280 Re_s \frac{d}{L} \left(\theta - \theta_{th}\right)^n \tag{2}$$

where d is the mean grain diameter, L is the barchan length, θ_{th} is the threshold value of the Shields number for incipient motion, n is an exponent, $Re_s = \rho U_s d/\mu$, and V_{ref} $= ((S-1)gd)^{1/2}$, with $S = \rho_s/\rho$ and U_s the settling velocity of particles. For water flows not far from the bedload threshold, Franklin and Charru (2011) found that $n = 5/2$, while the classical value for similar relations is $n = 3/2$, which have proven to work well for aeolian dunes (Bagnold, 1941), usually far from the threshold. Therefore, by assuming that $n = 3/2$ far from threshold, Eq. 2 implies that $V_d \sim d$. Close to the threshold and in turbulent regime, $(\theta - \theta_{th})^n$ is of lower asymptotic order than d^{-n}, since θ_{th} is an unknown function of d. Therefore, $V_d \sim d^a$, $a > 0$. By assuming that $a \approx 1$ for the subaqueous case (in order to match the aeolian scaling), both cases give $V_d \sim d$. In fact, we observe in our experiments that, all else being fixed, dunes composed of larger particles move faster, with V_d varying approximately with d. We note that Eq. 2 was obtained by Franklin and Charru (2011) for Re of the order of 10^4 ($13900 \leq Re \leq 23100$), 0.12 mm $\leq d \leq$ 0.51 mm, $1 \leq Re_* \leq 11$, and $\rho_p = 2600$ and 3760 kg/m^3, which are limited conditions, mainly in terms of Re and Re_*. Because in the present experiments Re_* varies within 3 and 10 (typical of the subaqueous case), Eq. 2 is clearly valid for our data. However, Eq. 2 may be improper for higher values of Re_*, having a different dependency on Re_s and changing the value of the exponent a, which might even assume negative values.

Observing that the diameter of the initial pile D is proportional to L, and considering the mean diameter and density as in Alvarez et al. (2021), $\bar{d} = \left(\phi_1/d_1 + \phi_2/d_2\right)^{-1}$ and $\bar{\rho}_s = \phi_1\rho_1 + \phi_2\rho_2$, respectively, we obtain

$$\Delta V_d \sim u_* \left| \frac{\bar{d}_t}{D_t} - \frac{\bar{d}_i}{D_i} \right| \frac{1}{S} \tag{3}$$

where $\bar{d}_i$ and $\bar{d}_t$ represent the mean diameter of grains forming impact and target barchans, respectively, and D_i and D_t are the initial diameters of the projected areas of impact and target bedforms, respectively. Finally,

$$t_s = \frac{\Delta x_d S}{u_*} \left| \frac{\bar{d}_t}{D_t} - \frac{\bar{d}_i}{D_i} \right|^{-1} \tag{4}$$

By normalizing the time interval that barchans take to complete their interaction Δt by the proposed timescale t_s, we obtain the characteristic time for interactions $t_c = \Delta t/t_s$ (values shown in Table 1). The initial instant for Δt is when the flow starts and the final instant when the interaction reaches a stage characteristic of the considered pattern. In cases with collision (merging, exchange and fragmentation-exchange), the final instant is when collision takes place, and in cases without collision (chasing and fragmentation-chasing), the final time is much larger than the duration of tests and we consider Δt as tending to infinity. In general, we observe the following characteristic times for interactions:

- $0.04 \leq t_c < 2$ for cases with collisions, i.e., the merging, exchange, fragmentation-exchange (by considering also the one-species monodisperse barchans presented in Assis and Franklin (2020, 2021)) and the undefined patterns of the two-species monodisperse barchans;

- $t_c = \infty$ for the chasing and fragmentation-chasing patterns.

Because only cases n and o (two-species monodisperse barchans) present $t_c = 0.04 < 0.1$ and only one fragmentation-exchange pattern for one-species monodisperse barchans (Assis & Franklin, 2021) presents $t_c = 1.7 > 1$, we obtained, in general, that $t_c = O(0.1)$, where $O()$ stands for "order of magnitude". This characteristic time holds for the barchans of same monodisperse composition (one species) presented in Assis and Franklin (2020, 2021), for the barchans consisting of bidisperse mixtures, and for the barchans consisting of different monodisperse grains.

The proposed timescale was verified only for subaqueous barchans, which present differences in the fundamental transport mechanism (bedload) when compared to aeolian dunes. Under water, the grains are entrained directly by the fluid and move by rolling and sliding, traveling distances of some grain diameters (between resting times), while in a gaseous environment they effectuate ballistic flights in the main flow direction over distances much larger than the grain diameter. In addition, the timescale is based on Eq. 2, which is valid for the subaqueous case, but not necessarily for other environments. However, the timescale that we propose is based on physical arguments, being basically the initial separation of barchans divided by their relative velocity. Therefore, although we cannot directly evaluate the timescale in other environments for which long-time measurements do not exist, we believe that it remains a reasonable reference. If the proposed timescale proves to be valid for other environments, it will allow the prediction of durations of barchan-barchan interactions and, more generally, provide a scaling for the evolution of dune fields on terrestrial deserts and other planetary environments.

The effect of polydisperse grains on barchan-barchan interactions and the existence of a proper timescale are two questions that were unexplored until now. In this paper, we investigated these issues by using bidisperse grains in a water channel. Other than the observation of a stratification process already reported by Alvarez et al. (2021) in the case of single dunes, we showed, for the first time, that the interaction patterns vary with grain concentrations, and that different interactions exist when each barchan consists of different monodisperse grains. In addition, we found the conditions for a collision in which the upstream barchan is larger than the downstream one, and we propose a timescale for the interactions of both monodisperse and bidisperse barchans. Our results shed light on those two questions, even if our findings remain to be investigated in other environments.

4 Conclusions

In this paper, we investigated experimentally the dune-dune interactions for barchans consisting of (i) bidisperse mixtures and (ii) different monodisperse grains (one type for each barchan). The experiments were conducted in a water channel where two barchans interacted with each other while filmed by a camera, and the bedform morphologies and duration of interactions were obtained from image processing. We observed that a transient stripe appears over the dunes in cases of bidisperse mixtures, as also happens for single bidisperse barchans (Alvarez et al., 2021). We showed, for the first time, that interaction patterns vary with grain concentrations, and that different interactions exist when each barchan consists of different monodisperse grains (two-species monodisperse barchans). For the latter, we obtained one very peculiar and unreported case by using larger grains in the impact barchan: the collision of a larger upstream barchan with a smaller downstream one, which showed a different grain distribution in the resulting bedform once the collision had taken place. Finally, we proposed a timescale for the interactions of both monodisperse and bidisperse barchans (cases i and ii, and also one-species monodisperse barchans). The identification of such timescale represents a new step for predicting the duration of binary interactions and, more generally, scaling the evolution of dune fields on Earth, Mars and other planetary environments.

Open Research

Data (digital images) supporting this work were generated by ourselves and are available in Mendeley Data (Assis et al., 2021) under the CC-BY-4.0 license. The numerical scripts used to process the images are also available in Mendeley Data (Assis et al., 2021) under the CC-BY-4.0 license.

Acknowledgments

The authors are grateful to FAPESP (Grant Nos. 2016/18189-0, 2018/14981-7 and 2019/10239-7) for the financial support provided.

References

Alvarez, C. A., Cúñez, F. D., & Franklin, E. M. (2021). Growth of barchan dunes of bidispersed granular mixtures. *Phys. Fluids*, *33*(5), 051705.

Alvarez, C. A., & Franklin, E. M. (2017, Dec). Birth of a subaqueous barchan dune. *Phys. Rev. E*, *96*, 062906. Retrieved from `https://link.aps.org/doi/10.1103/PhysRevE.96.062906` doi: 10.1103/PhysRevE.96.062906

Assis, W. R., Cúñez, F. D., & Franklin, E. M. (2021). Experimental data on barchan-barchan interaction with bidisperse grains [Dataset][Software]. *Mendeley Data, http://dx.doi.org/10.17632/sbjtzbzh9k*. doi: 10.17632/sbjtzbzh9k

Assis, W. R., & Franklin, E. M. (2020). A comprehensive picture for binary interactions of subaqueous barchans. *Geophys. Res. Lett.*, *47*(18), e2020GL089464.

Assis, W. R., & Franklin, E. M. (2021). Morphodynamics of barchan-barchan interactions investigated at the grain scale. *J. Geophys. Res.: Earth Surf.*, *126*(8), e2021JF006237.

Bacik, K. A., Lovett, S., Caulfield, C.-c. P., & Vriend, N. M. (2020, Feb). Wake induced long range repulsion of aqueous dunes. *Phys. Rev. Lett.*, *124*, 054501. Retrieved from `https://link.aps.org/doi/10.1103/PhysRevLett.124.054501` doi: 10.1103/PhysRevLett.124.054501

Bagnold, R. A. (1941). *The physics of blown sand and desert dunes*. London: Chapman and Hall.

Bo, T. L., & Zheng, X. J. (2013). Collision behaviors of barchans in aeolian dune fields. *Environ. Earth. Sci.*, *70*, 2963-2970.

Bristow, N. R., Blois, G., Best, J. L., & Christensen, K. T. (2018). Turbulent flow structure associated with collision between laterally offset, fixed-bed barchan dunes. *J. Geophys. Res.-Earth*, *123*(9), 2157-2188.

Bristow, N. R., Blois, G., Best, J. L., & Christensen, K. T. (2019). Spatial scales of turbulent flow structures associated with interacting barchan dunes. *J. Geophys. Res.-Earth*, *124*(5), 1175-1200.

Bristow, N. R., Blois, G., Best, J. L., & Christensen, K. T. (2020). Secondary flows and vortex structure associated with isolated and interacting barchan dunes. *J. Geophys. Res.-Earth*, *125*(2), e2019JF005257.

Claudin, P., & Andreotti, B. (2006). A scaling law for aeolian dunes on Mars, Venus, Earth, and for subaqueous ripples. *Earth Plan. Sci. Lett.*, *252*, 20-44.

Crocker, J. C., & Grier, D. G. (1996). Methods of digital video microscopy for colloidal studies. *Journal of Colloid and Interface Science*, *179*(1), 298-310.

Durán, O., Schwämmle, V., & Herrmann, H. (2005, Aug). Breeding and solitary wave behavior of dunes. *Phys. Rev. E*, *72*, 021308. Retrieved from `https://link.aps.org/doi/10.1103/PhysRevE.72.021308` doi: 10.1103/PhysRevE.72.021308

Durán, O., Schwämmle, V., Lind, P. G., & Herrmann, H. (2009). The dune size distribution and scaling relations of barchan dune fields. *Granular Matter*, *11*, 7-11.

Elbelrhiti, H., Andreotti, B., & Claudin, P. (2008). Barchan dune corridors: Field characterization and investigation of control parameters. *Journal of Geophysical Research: Earth Surface*, *113*(F2).

Elbelrhiti, H., Claudin, P., & Andreotti, B. (2005). Field evidence for surface-wave-induced instability of sand dunes. *Nature*, *437*(04058).

Endo, N., Taniguchi, K., & Katsuki, A. (2004). Observation of the whole process of interaction between barchans by flume experiments. *Geophys. Res. Lett.*, *31*(12).

Franklin, E. M., & Charru, F. (2009). Morphology and displacement of dunes in a closed-conduit flow. *Powder Technology*, *190*, 247-251.

Franklin, E. M., & Charru, F. (2011). Subaqueous barchan dunes in turbulent shear flow. Part 1. Dune motion. *J. Fluid Mech.*, *675*, 199-222.

Gay, S. P. (1999). Observations regarding the movement of barchan sand dunes in the nazca to tanaca area of southern peru. *Geomorphology*, *27*(3), 279 - 293.

Génois, M., du Pont, S. C., Hersen, P., & Grégoire, G. (2013). An agent-based model of dune interactions produces the emergence of patterns in deserts. *Geophys. Res. Lett.*, *40*(15), 3909-3914.

Génois, M., Hersen, P., du Pont, S., & Grégoire, G. (2013). Spatial structuring and size selection as collective behaviours in an agent-based model for barchan fields. *Eur. Phys. J. B*, *86*(447).

Groh, C., Rehberg, I., & Kruelle, C. A. (2009). How attractive is a barchan dune? *New J. Phys.*, *11*(2), 023014.

Herrmann, H. J., & Sauermann, G. (2000). The shape of dunes. *Physica A (Amsterdam)*, *283*, 24-30.

Hersen, P. (2004). On the crescentic shape of barchan dunes. *Eur. Phys. J. B*, *37*(4), 507–514.

Hersen, P., Andersen, K. H., Elbelrhiti, H., Andreotti, B., Claudin, P., & Douady, S. (2004, Jan). Corridors of barchan dunes: Stability and size selection. *Phys. Rev. E*, *69*, 011304. Retrieved from `https://link.aps.org/doi/10.1103/PhysRevE.69.011304` doi: 10.1103/PhysRevE.69.011304

Hersen, P., & Douady, S. (2005). Collision of barchan dunes as a mechanism of size regulation. *Geophys. Res. Lett.*, *32*(21).

Hersen, P., Douady, S., & Andreotti, B. (2002, Dec). Relevant length scale of barchan dunes. *Phys. Rev. Lett.*, *89*, 264301. Retrieved from `https://link.aps.org/doi/10.1103/PhysRevLett.89.264301` doi: 10.1103/PhysRevLett.89.264301

Hugenholtz, C. H., & Barchyn, T. E. (2012). Real barchan dune collisions and ejections. *Geophys. Res. Lett.*, *39*(2).

Katsuki, A., Kikuchi, M., Nishimori, H., Endo, N., & Taniguchi, K. (2011). Cellular model for sand dunes with saltation, avalanche and strong erosion: collisional simulation of barchans. *Earth Surf. Process. Landforms*, *36*(3), 372-382.

Katsuki, A., Nishimori, H., Endo, N., & Taniguchi, K. (2005). Collision dynamics of two barchan dunes simulated using a simple model. *J. Phys. Soc. Jpn.*, *74*(2), 538-541.

Kocurek, G., Ewing, R. C., & Mohrig, D. (2010). How do bedform patterns arise? new views on the role of bedform interactions within a set of boundary conditions. *Earth Surf. Process. Landforms*, *35*(1), 51-63.

Lima, A., Sauermann, G., Herrmann, H., & Kroy, K. (2002). Modelling a dune field. *Physica A*, *310*(3), 487-500. Retrieved from `https://www.sciencedirect.com/science/article/pii/S0378437102005460`

Norris, R. M., & Norris, K. S. (1961). Algodones Dunes of Southeastern California. *GSA Bulletin*, *72*(4), 605-619.

Parteli, E., & Herrmann, H. (2003). A simple model for a transverse dune field. *Physica A*, *327*(3), 554-562.

Parteli, E. J. R., & Herrmann, H. J. (2007, Oct). Dune formation on the present

618 mars. *Phys. Rev. E*, *76*, 041307. Retrieved from `https://link.aps.org/doi/`
619 `10.1103/PhysRevE.76.041307` doi: 10.1103/PhysRevE.76.041307
620 Schlichting, H. (2000). *Boundary-layer theory.* New York: Springer.
621 Schwämmle, V., & Herrmann, H. J. (2003). Solitary wave behaviour of sand dunes.
622 *Nature*, *426*, 619-620.
623 Vermeesch, P. (2011). Solitary wave behavior in sand dunes observed from space.
624 *Geophys. Res. Lett.*, *38*(22).
625 Zheng, X. J., Bo, T. L., & Zhu, W. (2009). A scale-coupled method for simulation
626 of the formation and evolution of aeolian dune field. *Int. J. Nonlinear Sci. Nu-*
627 *mer. Simul.*, *10*(3), 387-396.
628 Zhou, X., Wang, Y., & Yang, B. (2019). Three-dimensional numerical simulations of
629 barchan dune interactions in unidirectional flow. *Particul. Sci. Technol.*, *37*(7),
630 835-842.